Review Article

Quantitative sodium magnetic resonance imaging of cartilage, muscle, and tendon

Neal K. Bangerter[1,2], Grayson J. Tarbox[1], Meredith D. Taylor[1], Joshua D. Kaggie[3]

[1]Department of Electrical & Computer Engineering, Brigham Young University, Provo, UT, USA; [2]Department of Radiology, University of Utah, Salt Lake City, UT, USA; [3]Department of Radiology, University of Cambridge, Cambridge, UK

Correspondence to: Dr. Neal K. Bangerter. Department of Electrical & Computer Engineering, Brigham Young University, Provo, UT, USA. Email: nealb@ee.byu.edu.

Abstract: Sodium magnetic resonance imaging (MRI), or imaging of the 23Na nucleus, has been under exploration for several decades, and holds promise for potentially revealing additional biochemical information about the health of tissues that cannot currently be obtained from conventional hydrogen (or proton) MRI. This additional information could serve as an important complement to conventional MRI for many applications. However, despite these exciting possibilities, sodium MRI is not yet used routinely in clinical practice, and will likely remain strictly in the domain of exploratory research for the coming decade. This paper begins with a technical overview of sodium MRI, including the nuclear magnetic resonance (NMR) signal characteristics of the sodium nucleus, the challenges associated with sodium MRI, and the specialized pulse sequences, hardware, and reconstruction techniques required. Various applications of sodium MRI for quantitative analysis of the musculoskeletal system are then reviewed, including the non-invasive assessment of cartilage degeneration *in vivo*, imaging of tendinopathy, applications in the assessment of various muscular pathologies, and assessment of muscle response to exercise.

Keywords: Quantitative magnetic resonance imaging (quantitative MRI); musculoskeletal magnetic resonance imaging (musculoskeletal MRI); sodium magnetic resonance imaging (sodium MRI)

Submitted Nov 02, 2016. Accepted for publication Dec 03, 2016.
doi: 10.21037/qims.2016.12.10
View this article at: http://dx.doi.org/10.21037/qims.2016.12.10

Introduction

Proton, or 1H, magnetic resonance imaging (MRI) has revolutionized the ability to non-invasively image the human body over the past four decades. Proton MRI involves the excitation and reception of the nuclear magnetic resonance (NMR) signal of the hydrogen nucleus. Due to the widely varying chemical configurations and functional environments in which hydrogen is present in the human body, proton MRI is able to generate images with dozens of different contrasts. Images can be formed based on the relaxation properties of the NMR signal (1-4), diffusion characteristics of water molecules in a tissue (5-8), density of hydrogen nuclei, and a wide variety of other physiological and even functional tissue characteristics.

While 1H MRI is by far the most common MR imaging modality, sodium MRI, or imaging of the 23Na nucleus, has been under exploration for several decades for *in vivo* human imaging (9,10). Sodium MRI holds promise for potentially revealing additional biochemical information about the health of tissues, which could complement that obtained from 1H MRI. The concentrations and NMR signal characteristics of sodium nuclei in tissues could provide additional information about tissue viability, cell integrity, or even the abundance of other molecules whose presence is correlated with sodium concentration (11). However, despite these exciting possibilities, sodium MRI is not yet used routinely in clinical practice. Sodium imaging requires specialized hardware and software that is not currently available on the vast majority of clinical scanners. Furthermore, the ability to make quantitative measurements

from sodium images is hampered by comparatively poor image quality, long scan times (exacerbating patient motion and comfort concerns), low spatial resolutions, and complicated signal decay characteristics arising from the quadrupolar nature of the sodium nucleus (11,12).

Despite these challenges, recent advances in both gradient and radiofrequency coil hardware, the availability of whole-body scanners with higher main polarizing field strengths (3 Tesla and higher), and the development and refinement of ultra-short TE multi-nuclear pulse sequences have enabled significant advances in sodium MRI. *In vivo* sodium MRI is now being explored for applications ranging from the characterization and assessment of tumor viability (13,14), renal imaging (15,16), tissue damage following stroke (17), and myocardial imaging (18). One of the areas that shows particular promise for sodium MRI is imaging of musculoskeletal tissues, in particular muscle and cartilage. The loss of proteoglycan (PG) in cartilage is an early sign of cartilage degeneration, and portends the onset of osteoarthritis (OA) (19,20). Sodium concentration in cartilage has been shown to correlate directly with PG content, so the estimation of sodium concentration in cartilage from 23Na MRI images could serve as a non-invasive biomarker for cartilage degeneration.

In this work, we review the significant recent efforts to develop quantitative techniques for imaging and assessment of the musculoskeletal system using sodium MRI. We reviewed relevant literature found through both Google Scholar and PubMed searches for sodium MRI, and filtered these for musculoskeletal applications. We followed references in many of the landmark (most cited) papers in this area, and consulted several other review articles as well. Our references are selected based on what we feel is a fair and representative sample of the breadth of work in the area, and we were careful to include the most impactful articles in our references based on number of citations. The specific examples discussed and figures shown were selected from among the most prolific groups in musculoskeletal quantitative sodium MRI. The field is small enough that we believe we have provided a very thorough set of references.

We begin with a technical overview of sodium MRI, including the NMR signal characteristics of the sodium nucleus, the challenges associated with sodium MRI, and the specialized pulse sequences, hardware, and reconstruction techniques required. We then review the various applications of sodium MRI for quantitative analysis of the musculoskeletal system. These include the non-invasive assessment of cartilage degeneration *in vivo*, imaging of tendinopathy, applications in the assessment of various muscular pathologies, and assessment of muscle response to exercise.

Sodium MRI: technical overview

Challenges of sodium MRI

As previously mentioned, sodium MRI poses a variety of challenges that necessitate the use of specialized hardware and pulse sequences not available on most clinical scanners. These challenges also severely limit achievable spatial resolution and signal-to-noise ratio (SNR) when compared with traditional proton MRI. Challenges include (I) the rapid, bi-exponential decay of the sodium NMR signal in biological tissues arising from the 3/2 spin of the sodium nucleus; (II) the lower gyromagnetic ratio of sodium relative to hydrogen (γ_{Na} =11.26 MHz/T, approximately 1/4 that of hydrogen at γ_H =42.57 MHz/T); and (III) the significantly lower biological concentrations of 23Na *vs.* 1H.

Signal decay

The NMR signal decay of the spin 1/2 1H nucleus in many biological tissues of interest is well modeled by a single mono-exponential decay with time constant T2. For typical tissues directly visualized by proton MRI, T2 values range from approximately 25 ms to 2 s (21). This relatively slow decay of the proton NMR signal affords plenty of time for detection and sampling after signal excitation. Tissues that exhibit very short proton T2 decay time constants (tens of microseconds to maybe several milliseconds), such as tendon, ligament, and cortical bone, are typically MRI "invisible" due to the difficulty in detecting and sampling such a rapidly-decaying signal after excitation. These tissues show up as areas of signal void on most proton MR images.

In contrast to the 1H signal, the NMR signal from the 23Na nucleus (with spin 3/2) is well modeled by a bi-exponential decay (22) with both a short time constant $T2_{short}$ (often less than several milliseconds) and a longer time constant $T2_{long}$ (often 10–30 ms, which is quite short compared to hydrogen, but much longer than the short component) (11,23). The relative amplitudes of the short and long T2 components can vary significantly from tissue to tissue, and in biological tissues appear to be related to the fraction of intracellular *vs.* extracellular sodium (24-26). This relatively rapid and bi-exponential signal decay makes accurate detection of the sodium NMR signal more

challenging than that of 1H.

Lower gyromagnetic ratio

The lower gyromagnetic ratio of sodium (approximately 1/4 that of hydrogen) means that the sodium NMR signal is correspondingly lower than that of hydrogen. The NMR frequency is linearly proportional to the gyromagnetic ratio, and thus the sodium resonance frequency is approximately 1/4 that of hydrogen. At 3 Tesla, the hydrogen resonance is 127.71 MHz, while the sodium resonance is 33.78 MHz. Since the radiofrequency hardware in an MRI machine must be tuned to the resonant frequency of the nucleus to be imaged, this large disparity in resonant frequency requires that specialized radiofrequency hardware (including transmit and receive coils) be used for the excitation and detection of the sodium MRI signal. This specialized hardware is not present on most commercial MRI scanners.

Lower biological concentrations

Overall, sodium is approximately 10,000 times less abundant than hydrogen in the body (11). The NMR signal is proportional to the total number of signal-producing nuclei in the tissues being imaged. These much lower total concentrations of sodium lead to a much lower NMR signal, making signal detection with adequate SNR a significant challenge.

These challenges combine to make sodium MRI exceedingly difficult, and severely limit both spatial resolution and SNR achievable in clinically feasible scan times. Specialized software (pulse sequences) and hardware are required to make the acquisition of sodium images possible, as described below.

Pulse sequences for sodium MRI

There are a variety of pulse sequences that have been developed to enable the detection of the rapidly-decaying and bi-exponential sodium NMR signal. These pulse sequences need to (I) have a very short echo time TE (the time after signal excitation before the peak-amplitude NMR signal is sampled); and (II) have very short signal readout (sampling) duration. A very short TE is necessary to ensure that the sodium signal (particularly the short component) has not decayed away before the signal is sampled. Similarly, a very short signal readout duration helps to minimize signal decay during signal sampling. Signal decay during sampling leads to blurring in the final reconstructed images, which further complicates accurate quantitative measurement from the sodium signal.

Multiple quantum filtering

Multiple quantum filtered MR techniques have been explored for sodium imaging, and for attempting to distinguish between intracellular and extracellular sodium (27-29). However, these techniques suffer from very low SNR, and are challenging to use effectively *in vivo*. They have been largely supplanted for *in vivo* sodium MRI by the ultra-short echo time (UTE) sequences described below, so we will not devote time to describing or reviewing them. The interested reader is referred to previous publications (30-35).

3D radial techniques

As previously mentioned, a very short echo time TE and very short readout duration are desirable for sodium imaging. A straightforward way of achieving these goals is through the use of a 3D radial projection technique as shown in *Figure 1A* (36). Readout commences immediately after a hard non-selective RF pulse, and radial spokes emanating from the center of k-space are acquired, minimizing the readout duration required to achieve a given resolution. As samples are required on radial spokes and not on a Cartesian grid, a non-Cartesian reconstruction technique must be employed (39,40). This sequence is widely employed for *in vivo* sodium imaging.

Twisted projection imaging (TPI) and 3D cones

While the 3D radial technique described above can achieve very short TEs and the shortest readout durations possible for a desired resolution, they aren't as efficient in their ability to cover k-space as some other k-space trajectories. Two common variations employed for sodium MRI are TPI (37,41) and 3D cones imaging (38,42). In TPI, the trajectory starts out as simple 3D radial, but then begins to "twist" in k-space after a certain radius is surpassed in k-space (*Figure 1B*) (37). In 3D cones, k-space is sampled center-out on the surface of cones of changing azimuthal angle (*Figure 1C*) (38). Both of these trajectories allow the requisite k-space to be sampled with a smaller number of excitations than 3D radial, and make very efficient usage of gradient resources. While other techniques have been proposed (43-47), 3D radial techniques, 3D TPI, and 3D cones are currently the most commonly used pulse sequences for quantitative sodium MRI of the musculoskeletal system. 2D techniques are generally not used for sodium MRI because (I) slice selective excitations limit how short TE can be; and (II)

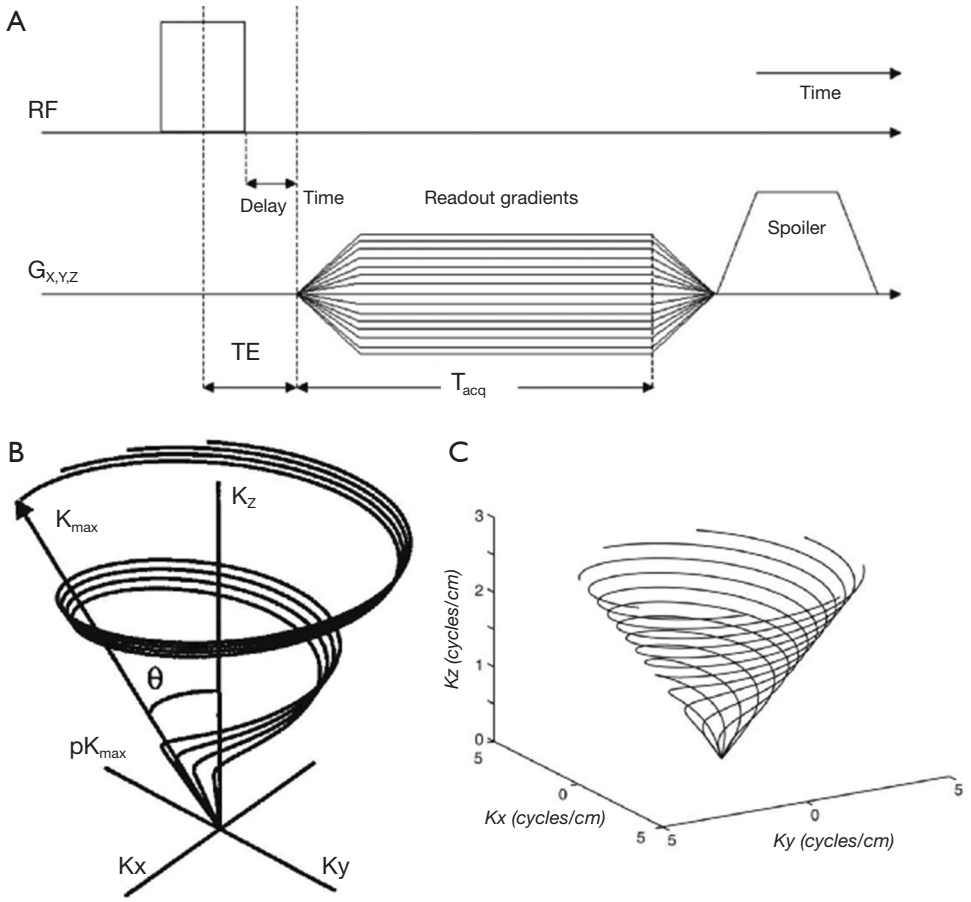

Figure 1 The pulse sequence diagram for a 3D radial project technique is shown in (A). In k-space, this trajectory corresponds to radial spokes emanating from the center of k-space (36). Copyright 2006 Wiley. Used with permission from Nielles-Vallespin S, Weber MA, Bock M, *et al.* 3D radial projection technique with ultrashort echo times for sodium MRI: Clinical applications in human brain and skeletal muscle. Magnetic Resonance in Medicine, John Wiley & Sons. The twisted projection imaging (TPI) k-space trajectory is shown in (B) (37). Copyright 1997 Wiley. Used with permission from Boada FE, Shen GX, Chang SY, *et al.* Spectrally weighted twisted projection imaging: reducing T2 signal attenuation effects in fast three-dimensional sodium imaging. Magnetic Resonance in Medicine, John Wiley & Sons. Finally the 3D cones k-space trajectory is shown in (C) (38). Copyright 2006 Wiley. Used with permission from Gurney PT, Hargreaves BA, Nishimura DG. Design and analysis of a practical 3D cones trajectory. Magnetic Resonance in Medicine, John Wiley & Sons.

long scan times and potentially multiple averages are needed to achieve adequate SNR, so 3D coverage of k-space is feasible in the required scan time and makes more efficient use of signal.

Pulse sequence parameters

While T1 for 1H in most biological tissues is between 300 ms and 4 s, T1 for sodium in biological tissues is relatively short (12–50 ms at 3 Tesla, and even shorter at 7 Tesla) (11,42,48,49). As a consequence, repetition time TR can be relatively short for sodium MR sequences while still achieving significant recovery of the longitudinal magnetization from TR to TR. Typical TR values are in the 40 to 100 ms range, although shorter TRs are sometimes used to attempt to achieve higher SNR efficiency (50). TE is generally made as short as possible—typically less than 400 microseconds—to capture as much of the rapidly decaying component of the sodium signal as possible. Readout durations are typically between 4 and 24 ms. These readout durations are long compared to $T2_{short}$, and thus significant T2 blurring is inevitable due to the rapid component of signal decay during readout. Unfortunately,

very short readout durations are impractical in sodium MRI for both SNR considerations (SNR is proportional to the square root of total readout duration) (51), and resolutions constraints (higher resolutions are achieved by sampling farther from the origin in k-space, which requires time). Finally, flip angles tend to be large if a TR greater than the estimated T1 is used. However, since T1 is not often precisely known for sodium experiments and because systems often have difficulty precisely calibrating the sodium flip angle, transmit gain is often simply adjusted to maximize sodium signal during prescan without precise knowledge of what the resulting flip angle is.

Sodium relaxometry

It is important to note that the straightforward application of the UTE sequences described above to sodium imaging yields a signal that is proportional to total tissue sodium concentration (TSC) in a tissue, since the UTE sequences effectively capture both short and long decay components of the sodium signal. While quantifying TSC is useful for many applications, these 3D UTE sequences can also be used for sodium relaxometry, such as sodium T2 mapping (52). It has even been demonstrated that sodium T2 mapping with a bi-exponential fit using 3D radial sequences can give relative fractions of short and long T2 decay in sodium without resorting to multiple quantum filtering techniques (53,54). However, these relaxometry techniques have found limited usage to date in musculoskeletal applications, as they typically require prohibitively long scan times for routine use.

Radiofrequency systems for sodium MRI

The much lower gyromagnetic ratio of 23Na compared to 1H results in a Larmor frequency that is approximately 1/4 that of 1H. The radiofrequency systems for an MRI system used for sodium must be capable of both exciting (transmitting) and receiving the lower frequency sodium signal. This typically involves the addition of a second broadband radiofrequency amplifier capable of exciting a broad range of frequencies other than that of 1H (so the amplifier can be used for a variety of other nuclei beyond 1H), as well as systems for signal reception and demodulation at other frequencies. The broadband amplifiers are typically much lower power than the main 1H RF amplifier, as the transmit coils used for signal excitation are typically much smaller than the 1H RF body coil built into the main bore of most 3 Tesla or lower whole-body scanners and consequently require much less power to excite the nuclei over a limited volume. Ultra-high field whole body systems, such as 7 Tesla systems, typically do not have a built-in body RF coil due to RF heating considerations; all signal excitation is done with smaller specialized transmit coils.

The radiofrequency systems described above are available from several major vendors as a scanner "multinuclear package" option or upgrade, but are not typically present on most clinical systems. In addition to the broadband transmit and reception hardware, radiofrequency coils (resonators) are needed for both signal excitation and reception at the appropriate frequency. These can be either a single coil that can operate both in transmit and receive modes (a "transmit/receive" or T/R coil), or separate coils. When a single T/R coil is used, an additional transmit/receive switch is needed as well, to first route the excitation RF signal through the T/R coil, and then to switch the electronics into receive mode during signal reception. A low-noise radiofrequency preamplifier tuned to the appropriate Larmor frequency is incorporated into the T/R switch. T/R switches often support both linear signal transmission and reception (single channel, suitable for simple single-loop radiofrequency coils and other linear coil designs) or quadrature transmission and reception (suitable for birdcage coils and other quadrature RF coil designs). Some modern systems may also support multi-channel reception at non-hydrogen frequencies to allow the use of non-hydrogen phased array receive coil designs.

While several of the major MRI vendors offer simple linear surface coil configurations at several non-hydrogen frequencies, most sodium imaging for musculoskeletal applications employs custom RF coils either produced in house or by one of several companies that design and build custom research MR coils. A variety of RF coil configurations for sodium imaging of the knee are shown in *Figure 2*. A four-ring dual-tuned 1H/23Na 3 Tesla knee coil is shown in *Figure 2A* (55). The inner two rings function as a low-pass birdcage resonator tuned to the sodium frequency, while the outer two rings function as a high-pass birdcage tuned to the hydrogen frequency. In *Figure 2B*, a 4-channel 23Na coil with a complete outer hydrogen-tuned birdcage surrounding it is shown (56), and in *Figure 2C*, an eight-channel 23Na coil with 4-channel proton for use at 7 Tesla is shown (57). Dual resonant coil designs such as these are attractive for sodium imaging, because they allow reference 1H images to be acquired without repositioning the subject.

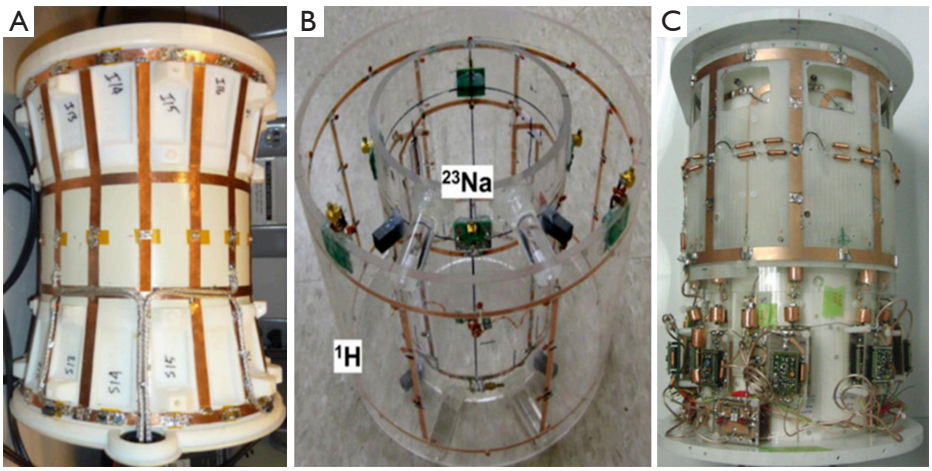

Figure 2 Three examples of dual-tuned 1H/23Na coils for knee imaging are shown. A four-ring dual-tuned 1H/23Na 3T knee coil is shown in (A) (55). Copyright 2010 Wiley. Used with permission from Asher K, Bangerter NK, Watkins RD, *et al*. Radiofrequency Coils for Musculoskeletal MRI, Topics in magnetic resonance imaging, John Wiley & Sons. The inner two rings function as a low-pass birdcage resonator tuned to the sodium frequency, while the outer two rings function as a high-pass birdcage tuned to the hydrogen frequency. In (B), a 4-channel 23Na coil with a complete outer hydrogen-tuned birdcage surrounding it is shown (56); and in (C), an 8-channel 23Na coil with 4-channel proton for use at 7 Tesla is shown (57). Copyright 2013 Wiley. Used with permission from Moon CH, Kim JH, Zhao T, *et al*. Quantitative 23Na MRI of human knee cartilage using dual-tuned 1H/23Na transceiver array radiofrequency coil at 7 tesla, Journal of Magnetic Resonance Imaging, John Wiley & Sons. Copyright 2012 Wiley. Used with permission from Brown R, Madelin G, Lattanzi R, *et al*. Design of a nested eight-channel sodium and four-channel proton coil for 7T knee imaging, Journal of Magnetic Resonance Imaging, John Wiley & Sons. Dual resonant coil designs such as these are attractive for sodium imaging, because they allow reference 1H images to be acquired without repositioning the subject.

Main polarizing field strength

Higher main polarizing field strengths yield a higher net magnetic polarization across tissues and a correspondingly higher signal without commensurate increases in noise, typically allowing higher SNR detection of the MR signal. This is particularly important in sodium imaging given low biological concentrations and lower sensitivity. *In vivo* (human) sodium MRI is now most commonly done on 3 and 7 Tesla whole-body systems.

Sodium MRI at very high fields (e.g., 7 Tesla) is actually in some ways easier than 1H imaging at these fields. The hydrogen resonance frequency is approximately 300 MHz at 7 Tesla, which yields a wavelength in many biological tissues of just 10–15 cm (often smaller than the anatomy being imaged). This is short enough that standing wave effects and skin depth become an issue in design of the RF transmit and receive coils. However, the sodium frequency at 7 Tesla is approximately 78 MHz, much closer to the hydrogen frequency at 1.5 Tesla (~64 MHz), where wavelengths in tissue are in the 40–60 cm range (larger than the dimensions of most anatomy being imaged). As a consequence, sodium imaging at 7 Tesla does not suffer from the difficulties arising from this much shorter wavelength (58).

Quantitative sodium MRI

A variety of useful quantitative measurements can theoretically be extracted from sodium MR images. The simplest is the measurement of sodium signal intensity (acquired with the shortest TE possible) normalized against a fiducial marker or markers of known sodium concentration as demonstrated in *Figure 3* (59). If a long TR (much greater than the sodium T1 of tissues being imaged) and short TE (much less than $T2_{short}$ of tissues being imaged), this normalized signal intensity is a good proxy for total TSC. However, it is important to note that this technique can be confounded by T1 variations across tissues when a TR is used that does not allow complete recovery to thermal equilibrium between excitations. That is, two tissues with the same total sodium concentration but different T1 may yield different normalized sodium signal

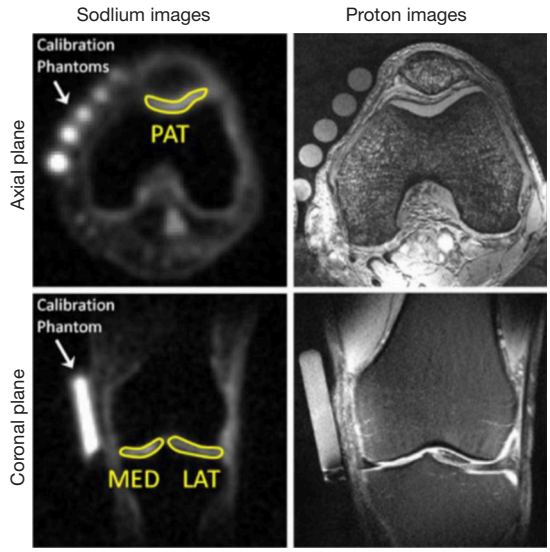

Figure 3 Fiducial phantoms of known sodium concentration and known sodium relaxation properties are often used to calibrate sodium concentration, as shown in these images from Madelin *et al*. (59). Copyright 2014 Wiley. Used with permission from Madelin G, Poidevin F, Makrymallis A, *et al*. Classification of sodium MRI data of cartilage using machine learning, Magnetic Resonance in Medicine, John Wiley & Sons.

intensity. In practice, the fiducial concentration markers are often designed to mimic the sodium relaxation properties of the tissue(s) of interest as close as possible.

More involved is the estimate of actual total TSC. This is done by mapping the sodium signal intensity to a concentration on a voxel-by-voxel basis by applying a signal model that may include estimates of T1, T2, and flip angle (60). In this case, fiducial markers of known sodium concentration and relaxation properties can be employed to provide reference signal levels. As previously mentioned, voxel-based sodium relaxometry is also being explored, including sodium T1 maps (52), sodium T2 maps (54), and even maps of $T2_{short}$ and $T2_{long}$ derived from bi-exponential fitting to sodium MR data taken at multiple echo times (53,54). Unfortunately, there are additional confounding factors that can decrease accuracy in the estimation of all of these quantitative measures.

First, inhomogeneity in flip angle across the volume being imaged (B1 inhomogeneity) will lead to signal variations not directly related to changes in sodium concentration or relaxation parameters. Significant error can be introduced due to B1 inhomogeneity in both normalized sodium signal intensity measures and estimates of TSC, although voxel-by-voxel relaxometry techniques are not as sensitive to B1 inhomogeneity across the volume. B1 mapping in sodium has been demonstrated (61), which could allow the inclusion of flip angle in the signal model on a voxel-by-voxel basis. However, the more common strategy is the use of a relatively homogeneous transmit coil (such as a quadrature birdcage) coupled with the assumption that variations in flip angle are small across the imaging volume. If surface or other highly inhomogeneous transmit coils are used, this is not feasible and B1 inhomogeneity must be included in the quantitative model. Similarly, inhomogeneity in receive coil sensitivity across the volume leads to spatial variations in sodium signal intensity not directly related to changes in sodium concentration or relaxation parameters. Like B1 inhomogeneity, receive coil sensitivity will directly affect quantitative measurement of normalized sodium signal intensity and estimation of TSC if not appropriately mapped and accounted for. But again, voxel-based relaxometry techniques are not as sensitive to these variations. Common strategies for dealing with receive coil sensitivity in quantitative sodium MRI include the use of very homogeneous receive coil geometries, or correction of signal intensities based on an estimated or measured receive coil sensitivity map.

Further errors in accurate quantitative measurement from sodium MRI arise from (I) signal loss from $T2_{short}$ decay due to the non-zero TE; (II) T2 blurring due to rapid signal decay during the readout; and (III) partial volume effects due to tissue mixing in relatively low-resolution voxels and exacerbated by T2 blurring across voxels. For example, in quantitative sodium MRI of cartilage, estimates of TSC in cartilage are confounded by sodium signal from synovial fluid adjacent to the cartilage (62,63). Fluid attenuated inversion recovery techniques have been demonstrated in sodium MRI to attempt to mitigate these partial-volume errors from synovial fluid (64,65).

Examples of quantitative sodium MRI for musculoskeletal applications

Assessing cartilage degeneration with sodium MRI

Degeneration of articular cartilage is associated with the progression of OA. A major component of articular cartilage is an extracellular matrix composed of water, collagen fibrils, and PG (66). PG depletion is one of the first signs of cartilage degeneration (67,68). Accurate measurement of

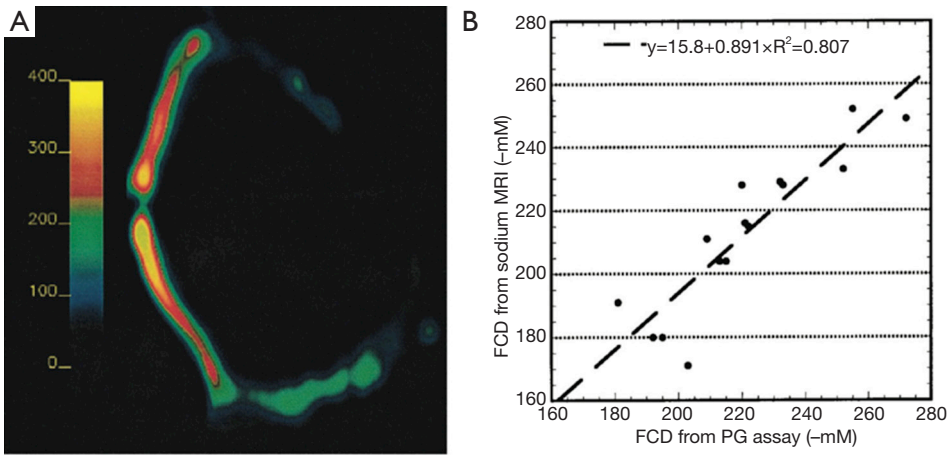

Figure 4 Shapiro *et al*. at University of Pennsylvania demonstrated that fixed charge density (FCD) as measured from sodium MRI correlates well with FCD measured from histological analysis (PG assay) (70). Copyright 2002 Wiley. Used with permission from Shapiro EM, Borthakur A, Gougoutas A, *et al*. 23Na MRI accurately measures fixed charge density in articular cartilage, Magnetic Resonance in Medicine, John Wiley & Sons. A sodium concentration map of a bovine patella (the top half of which was degraded by trypsin to reduce PG content) is shown on (A). On (B), the estimate of FCD as calculated from the sodium MRI images is compared to the density calculated from the PG assay, showing excellent agreement.

PG concentration in cartilage can be made *in vitro* through histology, but is more difficult to measure *in vivo*. PG create a fixed negative charge density in cartilage, and positively charged sodium ions are attracted to this negative charge and permeate the cartilage in concentrations proportional to the local PG concentration. Thus, concentrations of PG in cartilage can be inferred from sodium MRI by mapping TSCs in cartilage (69-74).

It should be noted that there are several other potentially promising techniques for assessing PG content in cartilage using 1H MRI. These include T1-rho imaging, gagCEST, and delayed gadolinium enhanced MRI of cartilage (dGEMRIC). While each of these techniques can readily be implemented on most standard commercial scanners, the relationship between the resulting image contrast and actual PG content is less straightforward than with sodium MRI (in the case of T1-rho and gagCEST imaging), or is theoretically less repeatable (in the case of dGEMRIC). The considerable interest in sodium MRI for assessing PG content in cartilage derives from its potential to be a much more direct and repeatable measure of PG content, provided sufficient SNR and resolution can be achieved.

Some of the first sodium images of articular cartilage were produced in the late 1980s by Granot (75). In the mid and late 1990s, Ravinder Reddy and colleagues at the University of Pennsylvania began applying multiple-quantum sodium MRI techniques to imaging of articular cartilage (33,34). The same laboratory did some of the early work in short TE sodium imaging of articular cartilage (66,76,77), and then went on to demonstrate that sodium MRI does indeed accurately measure fixed charge density (FCD) (and thus PG content), verified by histological analysis (70). Some results from this experiment are shown in *Figure 4*. A sodium concentration map of a bovine patella (the top half of which was degraded by trypsin to reduce PG content) is shown in *Figure 4A*. On *Figure 4B*, the estimate of FCD as calculated from the sodium MRI images is compared to the density calculated from the PG assay, showing excellent agreement.

Madelin, Regatte, Jerschow, and others at NYU continued to develop quantitative sodium MRI protocols for articular cartilage, measured sodium relaxation times in cartilage (48), introduced the previously-mentioned inversion recovery sodium protocol to mitigate partial volume affects from synovial fluid (64,65,78,79), and explored the reproducibility and repeatability of quantitative sodium MRI at 3 and 7 Tesla (64). 3D quantitative PG concentration maps (derived from 3D sodium MR images) of the knee acquired *in vivo* by the NYU group at both 3 and 7 Tesla are shown in *Figure 5*. Both the standard 3D radial sodium acquisition (top two rows, labeled R3D) and the group's inversion recovery sodium protocol (bottom two

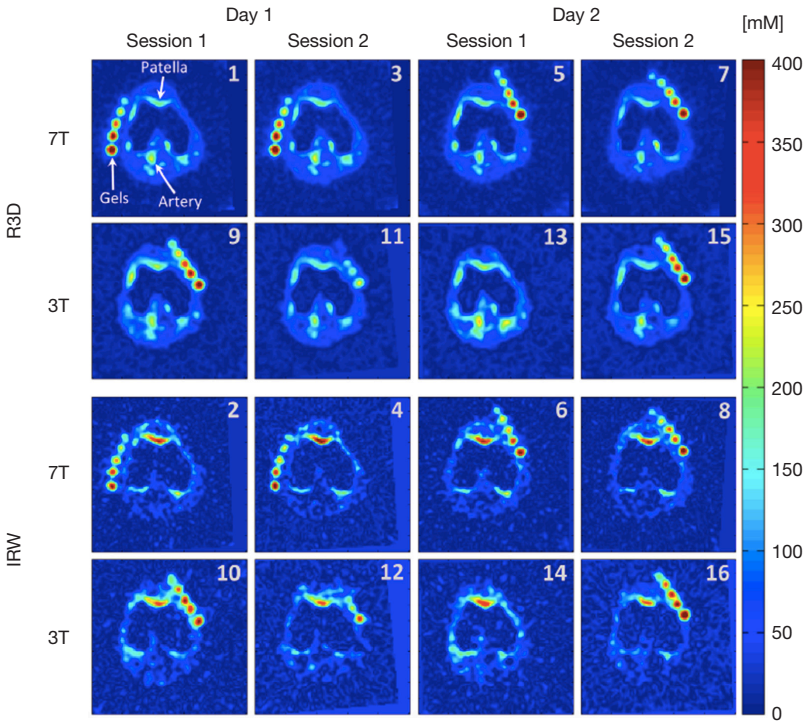

Figure 5 3D quantitative proteoglycan (PG) concentration maps (derived from 3D sodium MR images) of the knee acquired *in vivo* by Madelin *et al.* at NYU. Results are shown from both 3 and 7 Tesla. Both the standard 3D radial sodium acquisition (top two rows, labeled R3D) and the group's inversion recovery sodium protocol (bottom two rows, labeled IRW) were used, and imaging was repeated on the subject to assess repeatability (64). Copyright 2011 Wiley. Used with permission from Madelin G, Babb JS, Xia D, *et al.* Reproducibility and repeatability of quantitative sodium magnetic resonance imaging in vivo in articular cartilage at 3 T and 7 T, Magnetic Resonance in Medicine, John Wiley & Sons.

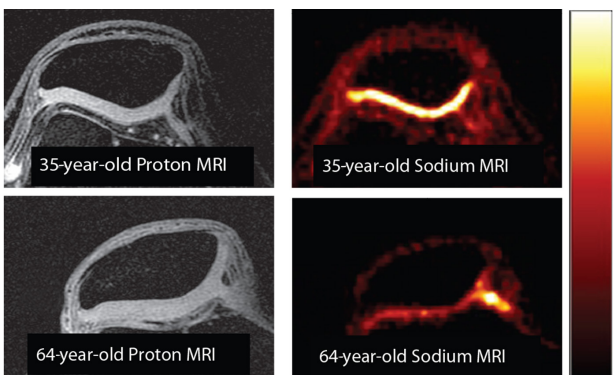

Figure 6 A demonstration of potentially age-related changes in proteoglycan (PG) content as revealed by high-resolution sodium MRI at 7 Tesla using a 3D cones sodium imaging sequence. While the cartilage looks healthy on both subjects in the proton images (left), there is a marked apparent decrease in sodium signal in the older subject (right). Images used courtesy of Stanford University Department of Radiology.

rows, labeled IRW) were used, and imaging was repeated on the subject to assess repeatability (64).

Staroswiecki *et al.* at Stanford demonstrated the first *in vivo* sodium images of articular cartilage using the 3D cones k-space trajectory at both 3 and 7 Tesla (80), and performed relaxometry measurements using 3D cones in knee cartilage (also at both 3 and 7 Tesla) (81). A demonstration of potentially age-related changes in PG content as revealed by high-resolution sodium MRI at 7 Tesla is shown in *Figure 6*, using the Stanford group's 3D cones sodium imaging sequence. Interesting recent work has improved upon quantitative sodium MRI protocols with an innovative RF coil design (56). Madelin *et al.* also have applied compressed sensing/constrained reconstruction techniques to sodium imaging of cartilage with good results (82). More recently, Madelin and others at NYU have done some interesting work on classification of sodium MRI data of cartilage using machine learning algorithms (59).

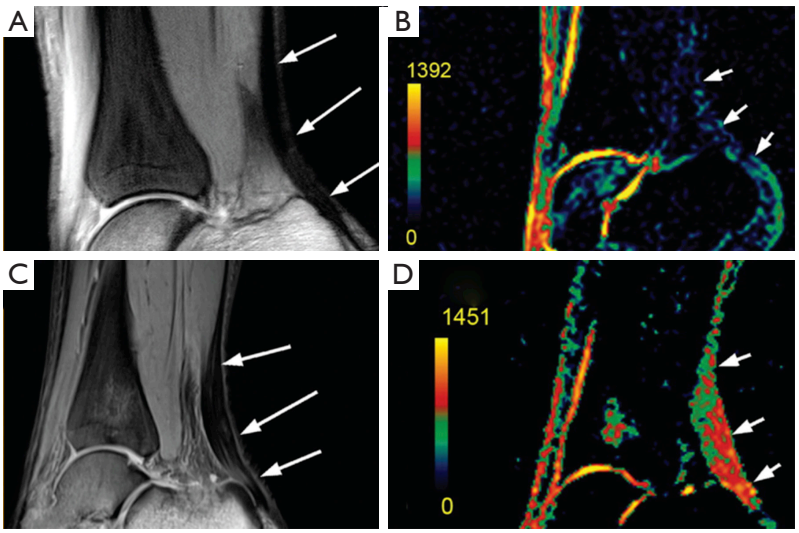

Figure 7 Proton (left) and sodium (right) scans of the Achilles tendon at 7 Tesla obtained by Juras *et al*. Results from a healthy 27-year-old control are shown in (A) (proton) and (B) (sodium), and a 46-year-old with chronic Achilles tendinopathy in (C) (proton) and (D) (sodium). A distinct increase in sodium signal in the subject with tendinopathy is clearly evident in these images (83). © The Radiological Society of North America. Reproduced with permission from Juras V, Zbýn S, Pressl C, *et al*. Radiology 2012;262:199-205.

Sodium imaging of tendon

Similar to cartilage, PG imparts a negative fixed-charge density to tendon, which in turn attracts positively charged sodium ions. Juras *et al*. hypothesize that decreases in PG content in pathologic tendons are likely to be accompanied by an increase in sodium content in the tendon, and that these increases in sodium content can be imaged with quantitative sodium MRI. They imaged the Achilles tendon of 20 healthy volunteers and 8 subjects with chronic Achilles tendinopathy at 7 Tesla using a 15-channel transmit/receive sodium knee coil. They found significant increases in sodium concentration in those suffering from Achilles tendinopathy *vs*. healthy controls (83). *Figure* 7 shows results from a healthy 27-year-old control in A (proton) and B (sodium), and a 46-year-old with chronic Achilles tendinopathy in C (proton) and D (sodium). A distinct increase in sodium signal in the subject with tendinopathy is clearly evident in these images.

Muscular channelopathies and muscular dystrophy

Sodium MRI has been explored as a potential diagnostic tool for the imaging of muscular diseases, such as muscular channelopathies and muscular dystrophy, which alter the normal distribution of intracellular and extracellular sodium ion concentration (84). Muscular channelopathies are caused by mutations in the sodium channels which lead to Na^+ accumulation in muscle (85). Muscular dystrophy also leads to increased sodium concentration in the muscle by altering sodium channel conductance (86). This suggests sodium MRI could be a potentially useful diagnostic tool for these diseases, although we are not aware of any studies to date that compare sodium MRI to other common (albeit more invasive) diagnostic tools such as muscle biopsy.

Both Amarteifio *et al*. and Nagel *et al*. performed similar studies comparing the sodium concentration in the calf muscles of patients with muscular channelopathies to healthy controls (85,87). Both studies were done at 3 Tesla, and used two scans to measure both total sodium content (using a T_1-weighted sodium image) and intracellular sodium content (using an inversion recovery sodium image). While they found differences in sodium content between patients with channelopathies and healthy volunteers on both sets of sodium images, the differences were more pronounced using the inversion recovery sequence. Weber *et al*. applied the same sodium MRI protocol at 3 Tesla to patients with muscular dystrophy and found that muscular dystrophy leads to differences in sodium concentration when compared to healthy controls (88,89). They also conclude that the sodium difference is mainly intracellular due to the greater difference seen on the inversion recovery sequence versus the T_1-weighted sodium image (*Figure 8*).

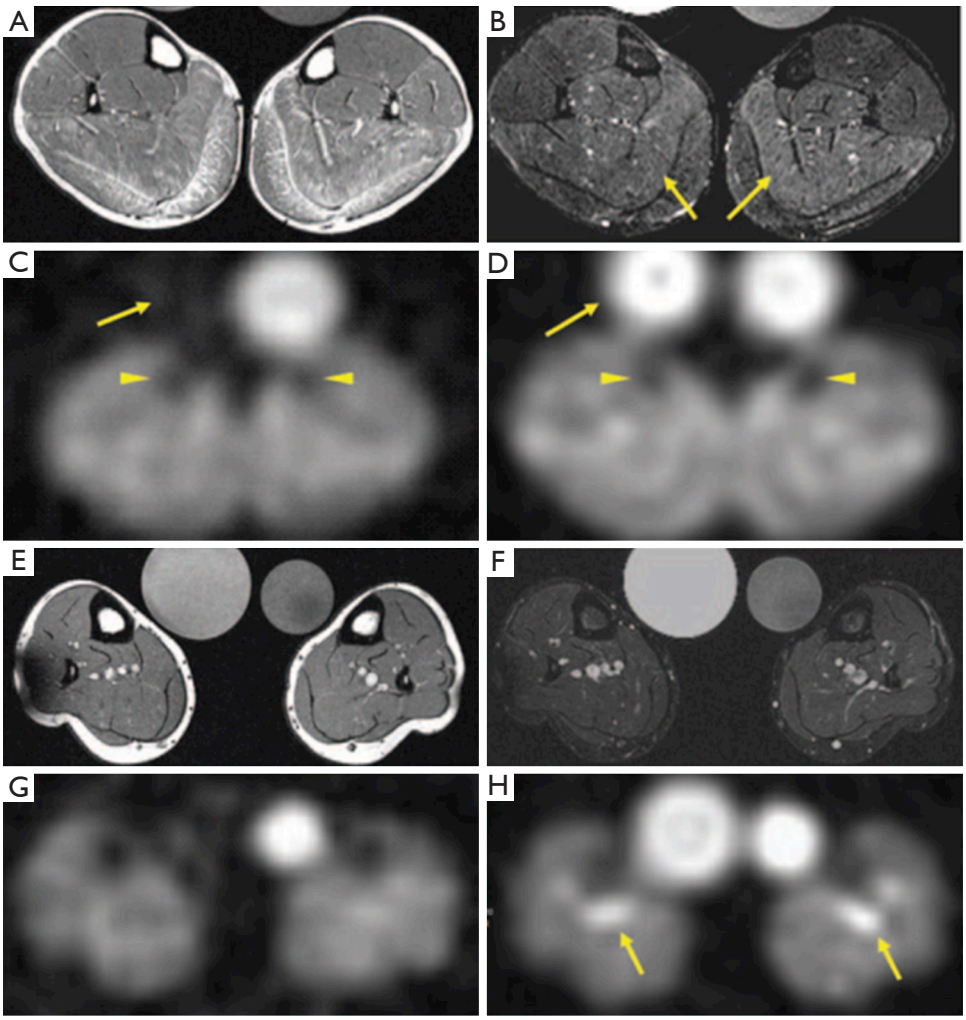

Figure 8 Weber *et al*. acquired images of a 10-year-old boy with Duchenne muscular dystrophy (A-D) and a 16-year-old healthy volunteer (E-H). 23Na IR (C) and tissue sodium concentration (TSC) 23Na MRI (D) show elevated levels of sodium in the soleus muscle of the boy with muscular dystrophy compared to the normal volunteer. A greater difference in sodium concentration is seen using the 23Na IR over total TSC suggesting the greater difference being in intracellular sodium concentration (88). Copyright 2011 Wolters Kluwer Heath, Inc. Used with permission from Weber MA, Nagel AM, Jurkat-Rott K, *et al*. Sodium (23Na) MRI detects elevated muscular sodium concentration in Duchenne muscular dystrophy, Neurology 2011;77:2017-24.

Muscle response to exercise

Studies have been performed to non-invasively examine muscle use during exercise based on the theory that possible fluid and electrolyte alterations in the extra- and intracellular compartments may produce changes in the 23Na NMR signal. While still at a very preliminary stage, sodium MRI could enable studies of muscle and exercise where invasive techniques like biopsy are undesired or impractical.

Other methods have been used to track muscle involvement in exercise, but quantitative 23Na MRI may offer some advantages over other methods. First, the sodium signal is sensitive to shifts in the relative sizes of the intra- and extracellular compartments since these compartments have widely differing sodium concentrations and are well-defined. Sodium concentration in the extracellular space is 145 mM, while concentration in the intracellular space is only 10–20 mM. Second, relaxation times for 23Na are very sensitive to the molecular environment in tissue due to

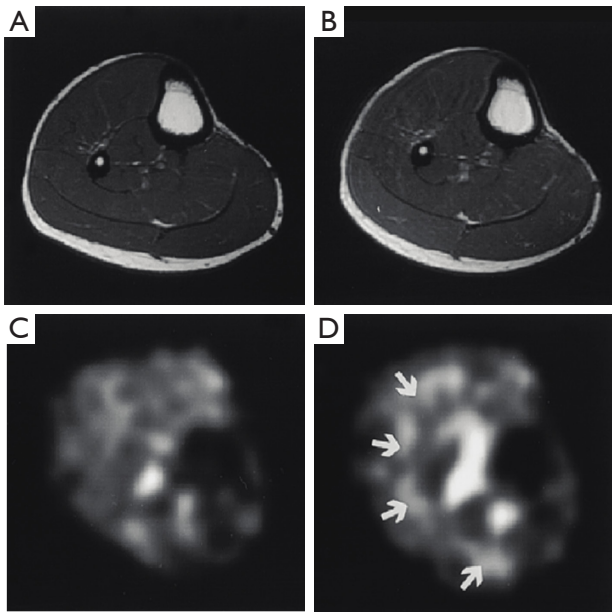

Figure 9 Constantinides *et al.* acquired transverse spin-echo T1-weighted MR images (TR/TE =800/25 ms) of the calf muscles of a healthy volunteer at baseline before exercise (A) and after a dynamic plantar flexion exercise protocol (B). The corresponding transverse 23Na images (TR/TE =55/0.37 ms, 0.22 mL voxels, total imaging time 16 minutes) obtained before (C) and after (D) exercise are also shown. Arrows in (D) indicate the regions of exercised, stressed, gastrocnemius and soleus muscle fibers (49).

quadrupole interactions. Under normal rest conditions, the extracellular space represents only 10–15% of the muscle volume, so even a small increase of extracellular volume would cause a notable increase in TSC (90,91). A change in the environment may also produce different sodium macromolecule interactions that could change the relaxation characteristics of the 23Na signal, causing a change in the signals from the $T2_{short}$ and $T2_{long}$ components.

Constantinides *et al.* investigated the effect of exercise on sodium concentration in calf muscle in 2000. Experiments were conducted at 1.5 Tesla using a TPI pulse sequence for image acquisition and a set of three vials containing known concentrations of sodium as fiducial markers. They noted an increase in signal intensity of 16% in the soleus muscle group and 22% in the gastrocnemius muscle group after exercise compared to the pre-exercise images. This sodium signal difference before and after exercise is shown in *Figure 9* (49). Bansal *et al.* conducted an independent investigation in the effects of exercise on the sodium signal in calf muscle around the same time as Constantinides in 2000. In addition to sodium concentration images (also collected at 1.5 Tesla), they acquired 23Na spectra and transverse relaxation times using a different imaging system at 1.9 Tesla. They found similar results indicating a 34% increase in signal intensity overall in exercised calf muscle *vs.* control. While the acquired spectra did not indicate a significant change in signal intensity following exercise, relaxation measurements indicated that the relative contribution of the short T2 component increased. They thus concluded that the changes in 23Na MRI signal intensity are largely attributed to a change in sodium macromolecular interaction rather than tissue sodium content (92). Recovery time for the sodium signal to return to a baseline pre-exercise level was also noted to have a half-life of 30 minutes.

Further investigation was conducted at 7 Tesla in 2010 by Chang *et al.* They noted a different signal intensity increase of 8–13% and a recovery time half-life of 12–15 minutes (93). They also compared the results of healthy volunteers to those who were diabetic, noting a similar increase in sodium intensity of 10–11%, but a longer recovery half-life of 27–37 minutes. Hammon *et al.* recently performed a similar study at 3 Tesla in both the calf and triceps muscles, and found similar changes in sodium signal intensity and concentration post exercise as previous investigators (94).

Summary and conclusions

Over the past 20 years, there has been significant progress in the acquisition of sodium MR images *in vivo* in reasonable scan times, and resolution and SNR has been steadily improving. While sodium images are of considerably lower SNR and quality than most 1H protocols, they have finally crossed a threshold where the resolutions and SNR are potentially suitable for accurate extraction of quantitative data from the images. This progress has been achieved through the development of highly SNR-efficient UTE MRI pulse sequences adapted for sodium imaging, improvements in gradient hardware, and improvements in radiofrequency coils for both exciting and receiving the sodium NMR signal. The use of higher main polarizing field strength magnets (3 and 7 Tesla) has also allowed the acquisition of higher quality sodium images. Building on this higher image quality, there has also been significant progress in extracting quantitative parameters (such as

total TSC, short and long T2 compartment fractions, and relaxometry measurements) using sodium MRI protocols.

Many of these improvements have been motivated by needs in musculoskeletal MRI. Quantitative sodium MRI protocols have now been successfully applied to quantifying PG content in articular cartilage as a marker of cartilage degeneration, imaging increased sodium concentrations in tendinopathy, observing deviations from the normal distributions of intracellular and extracellular sodium ion concentration resulting from muscular channelopathies and muscular dystrophy, and exploring muscle response to exercise.

However, it is important to note that the challenges associated with quantitative sodium MRI are considerable and there are a limited number of research centers currently capable of conducting such studies. In the authors' experience, much of the work done in quantitative sodium MRI at lower field strengths (1.5 and 3 Tesla) is limited to applications where relatively poor resolution (large voxel sizes) is acceptable. This is the case with some of the work in muscle. Repeatability is limited in applications with small feature size compared to voxel size, such as imaging of cartilage. At 7 Tesla, the resolution achievable with quantitative sodium MRI techniques is on the cusp of being acceptable for these applications that demand better resolution. We believe that the coming years will see an increase in the number of research centers pushing the capabilities of sodium MRI for musculoskeletal disorders, but actual clinical utilization is likely still more than a decade in the future.

Acknowledgements

None.

Footnote

Conflicts of Interest: The authors have no conflicts of interest to declare.

References

1. Koenig SH, Brown RD 3rd, Spiller M, Lundbom N. Relaxometry of brain: why white matter appears bright in MRI. Magn Reson Med 1990;14:482-95.
2. Deoni SC, Rutt BK, Peters TM. Rapid combined T1 and T2 mapping using gradient recalled acquisition in the steady state. Magn Reson Med 2003;49:515-26.
3. Deoni SC, Peters TM, Rutt BK. High-resolution T1 and T2 mapping of the brain in a clinically acceptable time with DESPOT1 and DESPOT2. Magn Reson Med 2005;53:237-41.
4. Cheng HL, Wright GA. Rapid high-resolution T(1) mapping by variable flip angles: accurate and precise measurements in the presence of radiofrequency field inhomogeneity. Magn Reson Med 2006;55:566-74.
5. Basser PJ, Jones DK. Diffusion-tensor MRI: theory, experimental design and data analysis - a technical review. NMR Biomed 2002;15:456-67.
6. Le Bihan D. Looking into the functional architecture of the brain with diffusion MRI. Nat Rev Neurosci 2003;4:469-80.
7. Le Bihan D, Poupon C, Amadon A, Lethimonnier F. Artifacts and pitfalls in diffusion MRI. J Magn Reson Imaging 2006;24:478-88.
8. Padhani AR, Liu G, Koh DM, Chenevert TL, Thoeny HC, Takahara T, Dzik-Jurasz A, Ross BD, Van Cauteren M, Collins D, Hammoud DA, Rustin GJ, Taouli B, Choyke PL. Diffusion-weighted magnetic resonance imaging as a cancer biomarker: consensus and recommendations. Neoplasia 2009;11:102-25.
9. Ra JB, Hilal SK, Oh CH, Mun IK. In vivo magnetic resonance imaging of sodium in the human body. Magn Reson Med 1988;7:11-22.
10. Turski PA, Perman WH, Houston L, Winkler SS. Clinical and experimental sodium magnetic resonance imaging. Radiol Clin North Am 1988;26:861-71.
11. Madelin G, Regatte RR. Biomedical applications of sodium MRI in vivo. J Magn Reson Imaging 2013;38:511-29.
12. Madelin G, Lee JS, Regatte RR, Jerschow A. Sodium MRI: methods and applications. Prog Nucl Magn Reson Spectrosc 2014;79:14-47.
13. Ouwerkerk R, Bleich KB, Gillen JS, Pomper MG, Bottomley PA. Tissue sodium concentration in human brain tumors as measured with 23Na MR imaging. Radiology 2003;227:529-37.
14. Ouwerkerk R, Jacobs MA, Macura KJ, Wolff AC, Stearns V, Mezban SD, Khouri NF, Bluemke DA, Bottomley PA. Elevated tissue sodium concentration in malignant breast lesions detected with non-invasive 23Na MRI. Breast Cancer Res Treat 2007;106:151-60.
15. Maril N, Rosen Y, Reynolds GH, Ivanishev A, Ngo L, Lenkinski RE. Sodium MRI of the human kidney at 3 Tesla. Magn Reson Med 2006;56:1229-34.
16. Rosen Y, Lenkinski RE. Sodium MRI of a human transplanted kidney. Acad Radiol 2009;16:886-9.
17. Thulborn KR, Davis D, Snyder J, Yonas H, Kassam A.

Sodium MR imaging of acute and subacute stroke for assessment of tissue viability. Neuroimaging Clin N Am 2005;15:639-53, xi-xii.
18. Constantinides CD, Kraitchman DL, O'Brien KO, Boada FE, Gillen J, Bottomley PA. Noninvasive quantification of total sodium concentrations in acute reperfused myocardial infarction using 23Na MRI. Magn Reson Med 2001;46:1144-51.
19. Matzat SJ, van Tiel J, Gold GE, Oei EH. Quantitative MRI techniques of cartilage composition. Quant Imaging Med Surg 2013;3:162-74.
20. Crema MD, Roemer FW, Marra MD, Burstein D, Gold GE, Eckstein F, Baum T, Mosher TJ, Carrino JA, Guermazi A. Articular cartilage in the knee: current MR imaging techniques and applications in clinical practice and research. Radiographics 2011;31:37-61.
21. Stanisz GJ, Odrobina EE, Pun J, Escaravage M, Graham SJ, Bronskill MJ, Henkelman RM. T1, T2 relaxation and magnetization transfer in tissue at 3T. Magn Reson Med 2005;54:507-12.
22. Rooney WD, Springer CS Jr. The molecular environment of intracellular sodium: 23Na NMR relaxation. NMR Biomed 1991;4:227-45.
23. Berendsen HJ, Edzes HT. The observation and general interpretation of sodium magnetic resonance in biological material. Ann N Y Acad Sci 1973;204:459-85.
24. Chang DC, Woessner DE. Spin-echo study of 23Na relaxation in skeletal muscle. Evidence of sodium ion binding inside a biological cell. Journal of Magnetic Resonance (1969) 1978;30:185-91.
25. Pettegrew JW, Woessner DE, Minshew NJ, Glonek T. Sodium-23 NMR analysis of human whole blood, erythrocytes, and plasma. Chemical shift, spin relaxation, and intracellular sodium concentration studies Journal of Magnetic Resonance (1969) 1984;57:185-96.
26. Cope FW. Spin-echo nuclear magnetic resonance evidence for complexing of sodium ions in muscle, brain, and kidney. Biophys J 1970;10:843-58.
27. Reddy R, Shinnar M, Wang Z, Leigh JS. Multiple-quantum filters of spin-3/2 with pulses of arbitrary flip angle. J Magn Reson B 1994;104:148-52.
28. Tsang A, Stobbe RW, Beaulieu C. Triple-quantum-filtered sodium imaging of the human brain at 4.7 T. Magn Reson Med 2012;67:1633-43.
29. Fleysher L, Oesingmann N, Inglese M. B_0 inhomogeneity-insensitive triple-quantum-filtered sodium imaging using a 12-step phase-cycling scheme. NMR Biomed 2010;23:1191-8.
30. Ooms KJ, Cannella M, Vega AJ, Marcolongo M, Polenova T. 23Na TQF NMR imaging for the study of spinal disc tissue. J Magn Reson 2008;195:112-5.
31. Navon G, Shinar H, Eliav U, Seo Y. Multiquantum filters and order in tissues. NMR Biomed 2001;14:112-32.
32. Borthakur A, Hancu I, Boada FE, Shen GX, Shapiro EM, Reddy R. In vivo triple quantum filtered twisted projection sodium MRI of human articular cartilage. J Magn Reson 1999;141:286-90.
33. Reddy R, Li S, Noyszewski EA, Kneeland JB, Leigh JS. In vivo sodium multiple quantum spectroscopy of human articular cartilage. Magn Reson Med 1997;38:207-14.
34. Reddy R, Insko EK, Leigh JS. Triple quantum sodium imaging of articular cartilage. Magn Reson Med 1997;38:279-84.
35. Eliav U, Shinar H, Navon G. The formation of a second-rank tensor in 23Na double-quantum-filtered NMR as an indicator for order in a biological tissue. Journal of Magnetic Resonance (1969) 1992;98:223-9.
36. Nielles-Vallespin S, Weber MA, Bock M, Bongers A, Speier P, Combs SE, Wöhrle J, Lehmann-Horn F, Essig M, Schad LR. 3D radial projection technique with ultrashort echo times for sodium MRI: clinical applications in human brain and skeletal muscle. Magn Reson Med 2007;57:74-81.
37. Boada FE, Shen GX, Chang SY, Thulborn KR. Spectrally weighted twisted projection imaging: reducing T2 signal attenuation effects in fast three-dimensional sodium imaging. Magn Reson Med 1997;38:1022-8.
38. Gurney PT, Hargreaves BA, Nishimura DG. Design and analysis of a practical 3D cones trajectory. Magn Reson Med 2006;55:575-82.
39. Beatty PJ, Nishimura DG, Pauly JM. Rapid gridding reconstruction with a minimal oversampling ratio. IEEE Trans Med Imaging 2005;24:799-808.
40. Fessler JA. On NUFFT-based gridding for non-Cartesian MRI. J Magn Reson 2007;188:191-5.
41. Boada FE, Gillen JS, Shen GX, Chang SY, Thulborn KR. Fast three dimensional sodium imaging. Magn Reson Med 1997;37:706-15.
42. Staroswiecki E, Nnewihe A, Bangerter NK, Daniel BL, Hargreaves BA. In Vivo Sodium Imaging and Relaxometry of the Breast at 3T. Proceedings of the 17th Annual Meeting of ISMRM; Honolulu, Hawaii, USA. 2009:2129.
43. Idiyatullin D, Corum C, Park JY, Garwood M. Fast and quiet MRI using a swept radiofrequency. J Magn Reson 2006;181:342-9.
44. Nagel AM, Laun FB, Weber MA, Matthies C, Semmler W, Schad LR. Sodium MRI using a density-adapted 3D radial

acquisition technique. Magn Reson Med 2009;62:1565-73.
45. Lu A, Atkinson IC, Claiborne TC, Damen FC, Thulborn KR. Quantitative sodium imaging with a flexible twisted projection pulse sequence. Magn Reson Med 2010;63:1583-93.
46. Pipe JG, Zwart NR, Aboussouan EA, Robison RK, Devaraj A, Johnson KO. A new design and rationale for 3D orthogonally oversampled k-space trajectories. Magn Reson Med 2011;66:1303-11.
47. Romanzetti S, Halse M, Kaffanke J, Zilles K, Balcom BJ, Shah NJ. A comparison of three SPRITE techniques for the quantitative 3D imaging of the 23Na spin density on a 4T whole-body machine. J Magn Reson 2006;179:64-72.
48. Madelin G, Jerschow A, Regatte RR. Sodium relaxation times in the knee joint in vivo at 7T. NMR Biomed 2012;25:530-7.
49. Constantinides CD, Gillen JS, Boada FE, Pomper MG, Bottomley PA. Human skeletal muscle: sodium MR imaging and quantification-potential applications in exercise and disease. Radiology 2000;216:559-68.
50. Newbould RD, Miller SR, Tielbeek JA, Toms LD, Rao AW, Gold GE, Strachan RK, Taylor PC, Matthews PM, Brown AP. Reproducibility of sodium MRI measures of articular cartilage of the knee in osteoarthritis. Osteoarthritis Cartilage 2012;20:29-35.
51. Nishimura DG. Principles of Magnetic Resonance Imaging. Lulu, 2016.
52. Kaggie JD, Park DJ, Newbould RD, Morrell GR, Hargreaves B, Staroswiecki E, Gold GE, Bangerter NK. In Vivo Breast Sodium T1 Measurements Using Inversion Recovery 3D Cones. Proceedings of the 19th Annual Meeting of ISMRM; Montreal, Quebec, Canada. 2011:3506.
53. Qian Y, Williams AA, Chu CR, Boada FE. Multicomponent T2* mapping of knee cartilage: technical feasibility ex vivo. Magn Reson Med 2010;64:1426-31.
54. Morrell G, Kaggie J, Stein M, Parker S, Bangerter N. Rapid high-resolution sodium relaxometry in human breast. Proceedings of the ISMRM 24th Annual Meeting; Singapore. 2016.
55. Asher KA, Bangerter NK, Watkins RD, Gold GE. Radiofrequency coils for musculoskeletal magnetic resonance imaging. Top Magn Reson Imaging 2010;21:315-23.
56. Moon CH, Kim JH, Zhao T, Bae KT. Quantitative (23) Na MRI of human knee cartilage using dual-tuned (1) H/(23) Na transceiver array radiofrequency coil at 7 tesla. J Magn Reson Imaging 2013;38:1063-72.
57. Brown R, Madelin G, Lattanzi R, Chang G, Regatte RR, Sodickson DK, Wiggins GC. Design of a nested eight-channel sodium and four-channel proton coil for 7T knee imaging. Magn Reson Med 2013;70:259-68.
58. Bangerter NK, Kaggie JD, Taylor MD, Hadley JR. Sodium MRI radiofrequency coils for body imaging. NMR Biomed 2016;29:107-18.
59. Madelin G, Poidevin F, Makrymallis A, Regatte RR. Classification of sodium MRI data of cartilage using machine learning. Magn Reson Med 2015;74:1435-48.
60. Christensen JD, Barrère BJ, Boada FE, Vevea JM, Thulborn KR. Quantitative tissue sodium concentration mapping of normal rat brain. Magn Reson Med 1996;36:83-9.
61. Allen SP, Morrell GR, Peterson B, Park D, Gold GE, Kaggie JD, Bangerter NK. Phase-sensitive sodium B1 mapping. Magn Reson Med 2011;65:1125-30.
62. Rong P, Regatte RR, Jerschow A. Clean demarcation of cartilage tissue 23Na by inversion recovery. J Magn Reson 2008;193:207-9.
63. Newbould RD, Miller SR, Upadhyay N, Rao AW, Swann P, Gold GE, Strachan RK, Matthews PM, Taylor PC, Brown AP. T1-weighted sodium MRI of the articulator cartilage in osteoarthritis: a cross sectional and longitudinal study. PLoS One 2013;8:e73067.
64. Madelin G, Babb JS, Xia D, Chang G, Jerschow A, Regatte RR. Reproducibility and repeatability of quantitative sodium magnetic resonance imaging in vivo in articular cartilage at 3 T and 7 T. Magn Reson Med 2012;68:841-9.
65. Madelin G, Lee JS, Inati S, Jerschow A, Regatte RR. Sodium inversion recovery MRI of the knee joint in vivo at 7T. J Magn Reson 2010;207:42-52.
66. Reddy R, Insko EK, Noyszewski EA, Dandora R, Kneeland JB, Leigh JS. Sodium MRI of human articular cartilage in vivo. Magn Reson Med 1998;39:697-701.
67. Bashir A, Gray ML, Burstein D. Gd-DTPA2- as a measure of cartilage degradation. Magn Reson Med 1996;36:665-73.
68. Bacic G, Liu KJ, Goda F, Hoopes PJ, Rosen GM, Swartz HM. MRI contrast enhanced study of cartilage proteoglycan degradation in the rabbit knee. Magn Reson Med 1997;37:764-8.
69. Lesperance LM, Gray ML, Burstein D. Determination of fixed charge density in cartilage using nuclear magnetic resonance. J Orthop Res 1992;10:1-13.
70. Shapiro EM, Borthakur A, Gougoutas A, Reddy R. 23Na MRI accurately measures fixed charge density in articular cartilage. Magn Reson Med 2002;47:284-91.
71. Wheaton AJ, Borthakur A, Shapiro EM, Regatte RR, Akella SV, Kneeland JB, Reddy R. Proteoglycan loss in human knee cartilage: quantitation with sodium MR

imaging--feasibility study. Radiology 2004;231:900-5.
72. Insko EK, Kaufman JH, Leigh JS, Reddy R. Sodium NMR evaluation of articular cartilage degradation. Magn Reson Med 1999;41:30-4.
73. Wheaton AJ, Borthakur A, Dodge GR, Kneeland JB, Schumacher HR, Reddy R. Sodium magnetic resonance imaging of proteoglycan depletion in an in vivo model of osteoarthritis. Acad Radiol 2004;11:21-8.
74. Borthakur A, Shapiro EM, Akella SV, Gougoutas A, Kneeland JB, Reddy R. Quantifying sodium in the human wrist in vivo by using MR imaging. Radiology 2002;224:598-602.
75. Granot J. Sodium imaging of human body organs and extremities in vivo. Radiology 1988;167:547-50.
76. Insko EK, Reddy R, Leigh JS. High resolution, short echo time sodium imaging of articular cartilage. J Magn Reson Imaging 1997;7:1056-9.
77. Borthakur A, Shapiro EM, Beers J, Kudchodkar S, Kneeland JB, Reddy R. Sensitivity of MRI to proteoglycan depletion in cartilage: comparison of sodium and proton MRI. Osteoarthritis Cartilage 2000;8:288-93.
78. Chang G, Madelin G, Sherman OH, Strauss EJ, Xia D, Recht MP, Jerschow A, Regatte RR. Improved assessment of cartilage repair tissue using fluid-suppressed ^{23}Na inversion recovery MRI at 7 Tesla: preliminary results. Eur Radiol 2012;22:1341-9.
79. Madelin G, Babb J, Xia D, Chang G, Krasnokutsky S, Abramson SB, Jerschow A, Regatte RR. Articular cartilage: evaluation with fluid-suppressed 7.0-T sodium MR imaging in subjects with and subjects without osteoarthritis. Radiology 2013;268:481-91.
80. Staroswiecki E, Bangerter NK, Gurney PT, Grafendorfer T, Gold GE, Hargreaves BA. In vivo sodium imaging of human patellar cartilage with a 3D cones sequence at 3 T and 7 T. J Magn Reson Imaging 2010;32:446-51.
81. Staroswiecki E, Bangerter N, Gurney PT, Gold G, Holdsworth SJ, Grafendorfer T, Hargreaves BA. In Vivo Measurement of 23 Na T2* in Human Articular Cartilage at 3T and 7T. Proc Intl Soc Mag Reson Med 2008;16:324.
82. Madelin G, Chang G, Otazo R, Jerschow A, Regatte RR. Compressed sensing sodium MRI of cartilage at 7T: preliminary study. J Magn Reson 2012;214:360-5.
83. Juras V, Zbýn S, Pressl C, Domayer SE, Hofstaetter JG, Mayerhoefer ME, Windhager R, Trattnig S. Sodium MR imaging of Achilles tendinopathy at 7 T: preliminary results. Radiology 2012;262:199-205.
84. Vilin YY, Ruben PC. Slow inactivation in voltage-gated sodium channels: molecular substrates and contributions to channelopathies. Cell Biochem Biophys 2001;35:171-90.
85. Amarteifio E, Nagel AM, Weber MA, Jurkat-Rott K, Lehmann-Horn F. Hyperkalemic periodic paralysis and permanent weakness: 3-T MR imaging depicts intracellular 23Na overload--initial results. Radiology 2012;264:154-63.
86. Kushnir T, Knubovets T, Itzchak Y, Eliav U, Sadeh M, Rapoport L, Kott E, Navon G. In vivo 23Na NMR studies of myotonic dystrophy. Magn Reson Med 1997;37:192-6.
87. Nagel AM, Amarteifio E, Lehmann-Horn F, Jurkat-Rott K, Semmler W, Schad LR, Weber MA. 3 Tesla sodium inversion recovery magnetic resonance imaging allows for improved visualization of intracellular sodium content changes in muscular channelopathies. Invest Radiol 2011;46:759-66.
88. Weber MA, Nagel AM, Jurkat-Rott K, Lehmann-Horn F. Sodium (23Na) MRI detects elevated muscular sodium concentration in Duchenne muscular dystrophy. Neurology 2011;77:2017-24.
89. Weber MA, Nagel AM, Wolf MB, Jurkat-Rott K, Kauczor HU, Semmler W, Lehmann-Horn F. Permanent muscular sodium overload and persistent muscle edema in Duchenne muscular dystrophy: a possible contributor of progressive muscle degeneration. J Neurol 2012;259:2385-92.
90. Sreter FA. Cell water, sodium, and potassium in stimulated red and white mammalian muscles. Am J Physiol 1963;205:1295-8.
91. Sjøgaard G, Adams RP, Saltin B. Water and ion shifts in skeletal muscle of humans with intense dynamic knee extension. Am J Physiol 1985;248:R190-6.
92. Bansal N, Szczepaniak L, Ternullo D, Fleckenstein JL, Malloy CR. Effect of exercise on (23)Na MRI and relaxation characteristics of the human calf muscle. J Magn Reson Imaging 2000;11:532-8.
93. Chang G, Wang L, Schweitzer ME, Regatte RR. 3D 23Na MRI of human skeletal muscle at 7 Tesla: initial experience. Eur Radiol 2010;20:2039-46.
94. Hammon M, Grossmann S, Linz P, Kopp C, Dahlmann A, Janka R, Cavallaro A, Uder M, Titze J. 3 Tesla (23)Na magnetic resonance imaging during aerobic and anaerobic exercise. Acad Radiol 2015;22:1181-90.

Cite this article as: Bangerter NK, Tarbox GJ, Taylor MD, Kaggie JD. Quantitative sodium magnetic resonance imaging of cartilage, muscle, and tendon. Quant Imaging Med Surg 2016;6(6):699-714. doi: 10.21037/qims.2016.12.10